

Measurements of momentum correlation and interaction parameters between antiprotons

Zheng-Qiao Zhang^{1,2} · Yu-Gang Ma¹

Received: 19 September 2016/Revised: 9 October 2016/Accepted: 9 October 2016/Published online: 2 November 2016
© Shanghai Institute of Applied Physics, Chinese Academy of Sciences, Chinese Nuclear Society, Science Press China and Springer Science+Business Media Singapore 2016

Abstract The two-particle momentum correlation is influenced by the nuclear force between two particles, which has been intensively studied for nucleons and nuclei, but not much for antinucleons or antinuclei. In this proceeding, we present our STAR measurements on momentum correlation function of antiproton–antiproton and proton–proton in Au+Au collisions at $\sqrt{s_{NN}} = 200$ GeV at the Relativistic Heavy Ion Collider. Attractive nuclear force between two antiprotons is demonstrated, and the strong interaction parameters (the scattering length and the effective range) are determined. This measurement serves as an additional verification of CPT symmetry. The present information on the strong force in the antiproton–antiproton system provides a fundamental ingredient towards understanding the structure of more sophisticated antinuclei.

Keywords Antiproton · Momentum correlation · Antimatter interaction · CPT symmetry

This work was supported in part by the National Natural Science Foundation of China (No. 11421505) and the Major State Basic Research Development Program in China (No. 2014CB845401).

✉ Yu-Gang Ma
ygma@sinap.ac.cn

¹ Shanghai Institute of Applied Physics, Chinese Academy of Sciences, Shanghai 201800, China

² University of Chinese Academy of Sciences, Beijing 100049, China

1 Introduction

Understanding the nucleon force is one of the main goals in nuclear physics [1, 2], which is a necessary step to understand the structure of nuclei. In addition, behaviors of antiparticles or antiparticle induced reactions are always of interest [3–5]. So far the large body of knowledge on nuclear force was derived from studies made on nucleons or nuclei, and not much is known about the nuclear force between antinucleons. The knowledge of interaction among two antiprotons, the simplest system of antinucleons (nuclei), is a fundamental ingredient for understanding the structure of more sophisticated antinuclei and their properties. The important parameters to describe the strong interaction between two particles are the scattering length (f_0) and the effective range of the interaction (d_0). The parameter f_0 is related to the scattering cross section. At low energy limit, the scattering cross section is given by $\sigma = 4\pi f_0^2$. The parameter d_0 is related to the range of the potential. In the case of square well potential, d_0 is the range (radius) of the potential. For a short range potential, f_0 and d_0 are related to the s-wave scattering phase shift, δ_0 , and the collision momentum, k , by $k \cot \delta_0 \approx 1/f_0 + \frac{1}{2}d_0k^2$. To illustrate the scattering length (f_0) and the effective range of the interaction (d_0) cleanly, we use a square potential as an example. Figure 1 shows the square potential and the wave functions corresponding to different setups. V_0 represents the potential, and r_0 is for the radius part of the wave function. Here $r_0 = d_0$, i.e., the effective range. In case (a) we have $V_0 > 0$ for a repulsive potential and the other three are attractive, with different depths. For square well potential, the effective range is the range (radius) of the potential, and a (or $-f_0$) is the intercept on the r

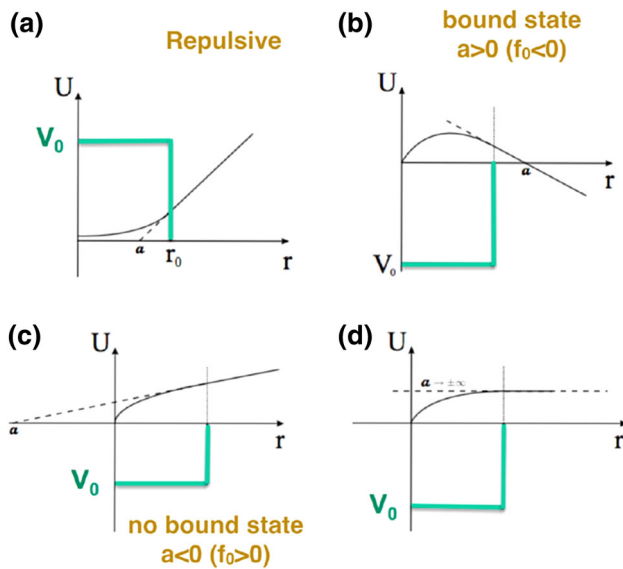


Fig. 1 (Color online) The square potential versus the wave functions corresponding to different setups. **a** repulsive potential; **b** attractive potential which can form the bound state; **c** attractive potential but no bound state; and **d** attractive potential with “zero energy resonance”

axis when one does a linear extrapolation of the wave function at the barrier. If a bound state can be formed, one needs an attractive potential and the maximum of the wave function inside the potential range, like case (b). However, in case (c) when $a < 0$ ($f_0 > 0$), no bound state will be formed even though the potential is still attractive. In case d), the a is divergent at infinite. This is a special case usually called “zero energy resonance”. Put it in short, for a bound state to be formed, one needs an attractive potential and $a > 0$ (or $f_0 < 0$).

Although the existence and production rates of anti-matter nuclei [6, 7] include antideuterons, antitritons, antihelium-3, antihypertriton [8–10], and antihelium-4 [8, 11, 12], offer indirect information about interactions between antinucleons. The interaction between two antinucleons, which is the basic interaction that binds the antinucleons into antinuclei, has not been directly measured in previous experiments. On the other hand, the measurement between antiprotons offers us a test of matter–antimatter symmetry, which is known as charge conjugation-parity transformation-time reversal (CPT) symmetry. Different CPT tests were conducted in other experiments. For example, one of which is the precious mass difference measurement for light nuclei and light antinuclei, such as deuteron and antideuteron, there is ${}^3\text{He}$ and anti- ${}^3\text{He}$ by the ALICE collaboration [13]. Another example is a high-precision comparison of the antiproton-to-proton charge-to-mass ratio carried out in a Penning trap system [14]. In this work we would test the CPT from strong interaction aspect which is the nuclear force [15].

Relativistic heavy-ion collision provides a unique environment for not only the formation of quark–gluon plasma (QGP) [16–18], but also the production of anti-matter nuclei [8]. With abundantly produced antiprotons, we can for the first time measure the scattering length (f_0) and the effective range (d_0) of the strong interaction between antinucleons. To do that, we use the technique that involves momentum correlation for probing the antiproton–antiproton interaction. It resembles the space-time correlation technique used in Hanbury-Brown and Twiss (HBT) intensity interferometry. Since it was first used in astronomy by Hanbury-Brown and Twiss in the 1950s [19], this technique [20–22] has been used in many areas of physics, including the study of the quantum state of Bose–Einstein condensates [23], the correlation among electrons [24], and among atoms in cold Fermi gases [25]. In the late 1950s, the Bose–Einstein enhancement, which is an enhanced number of pairs of identical pions produced with small opening angles, was first observed (GGLP effect) [26]. Later on, Kopylov and Podgoretsky devised the basics of the momentum correlation interferometry technique. In this technique, they defined the correlation functions (CFs) as ratios of the momentum distributions of correlated and uncorrelated particles,

$$C(\mathbf{p}_1, \mathbf{p}_2) = \frac{P(\mathbf{p}_1, \mathbf{p}_2)}{P(\mathbf{p}_1)P(\mathbf{p}_2)}, \quad (1)$$

with $C = 1$ for no correlations. One can apply the mixing technique to construct the uncorrelated distribution by using particles from different collisions and extracting the space-time structure of the particle emission from the correlation function. So far the method of momentum correlation has been widely used by the nuclear physics community [27–33]. In particular, the same technique can even be applied for the complete kinematically three body decay of the nuclei very recently, which is very powerful to investigate the proton emission mechanism [34, 35].

2 STAR experiment

The process of two-particle correlation can be illustrated in Fig. 2 at RHIC–STAR detector. Colorful tracks display the different charged particles which are recorded by the Time Projection Chamber (TPC) at STAR. Assuming both correlated two (anti)protons (red and yellow curves) are emitted from the source, they will interfere each other and finally produce intensity interferometry spectra, i.e., momentum correlation function. For each correlation function, in addition to quantum statistics effects, final state interactions (FSI) play an important role in the formation of correlations between particles. FSI includes the formation of resonances, the Coulomb repulsion, and the nuclear

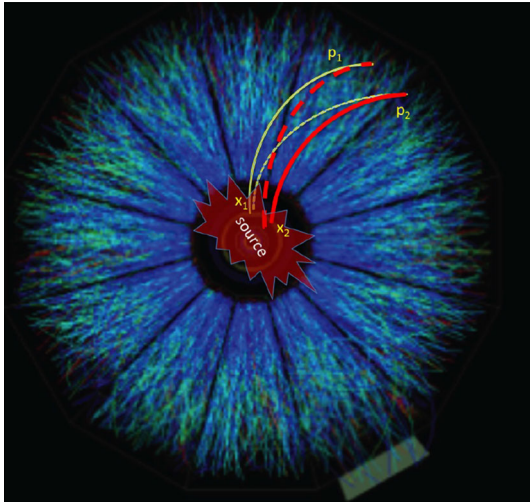


Fig. 2 (Color online) Demonstration of two-particle correlation in heavy-ion collisions from the TPC in the STAR detector. The *curves* show particle trajectories where the track momenta can be determined. The 3-vector momenta can be measured by STAR detector in a wide range from about 0.1 GeV/c. Two particles were emitted from two separated points, with four-coordinates, x_1 and x_2 . Their four-momenta, p_1 and p_2 , were detected

interactions between two particles, etc [27, 28, 36, 37]. They allows for (see Refs. [29, 38] and references therein) coalescence femtoscopy, correlation femtoscopy with nonidentical particles, including access to the relative space-time production asymmetries, and a measurement of the strong interaction between specific particles. The latter measurement is often difficult to access by other means and is the focus of this proceeding paper (for recent studies see Refs. [39, 40]).

The data used in this analysis are Au + Au minimum bias events taken by the STAR experiment at RHIC during year 2011 at center-of-mass energies $\sqrt{s_{NN}} = 200$ GeV. All data used here were taken by STAR Time Projection Chamber (TPC) [41] and Time of Flight detector (TOF) [42]. The TPC provides kinematic parameters of a track as well as the particle identification information based on the ionization energy loss. The TOF provides the mass information of the track. A Zero Degree Calorimeter (ZDC) [43] and a Vertex Position Detector (VPD) are combined to implement a minimum bias trigger. For event level, we use $|V_z| < 30$ cm, $|V_r| < 2$ cm and $|TPCV_z - VPDV_z| < 3$ cm. In our analysis, we select 30–80% centrality. A C++ class (StRefMultCorr) has been provided in STAR as a standard class to handle the centrality determination and generate event weight according to the centrality and luminosity at the same time. All centrality determination in this analysis is from the StRefMultCorr class. A set of basic track quality cuts used are listed in Table 1. A TPC track can have up to 45 hits, and a minimum of 15 TPC hits used in track fitting is required for every track participating the

Table 1 Basic track quality cuts

Cut parameter	Value
NHitsFit	≥ 15
NhitsFit/NHitsPoss	> 0.52
p_T	> 0.4 GeV/c
p_T	< 2.0 GeV/c
Rapidity	< 0.7
nSigma Proton	< 1.5
Mass square	< 0.8
Mass square	< 1.0
Global dca	< 2.0 cm

analysis. A single, long TPC track may be reconstructed as two shorter tracks if track splitting happens. These two short tracks have almost identical track parameters and only one of them should be used. Requiring the ratio of number of fitting hits over the number of maximum possible hits larger than 0.52 can effectively suppress the track splitting. A minimum transverse momentum of 0.4 GeV is required. The distance of closest approach (DCA) to primary vertex of global tracks is required to be smaller than 2 cm to select primary tracks. In order to select proton samples from the track, we use the nSigma cut and mass square cut. The information of the mass square can be derived from the TOF detector. Figure 3 shows a mass squared (m^2) distribution versus n_{σ_z} for antiprotons. By using both TPC and TOF, the purity for (anti)protons can be over $> 99\%$ with transverse momentum (p_T) less than 2 GeV/c.

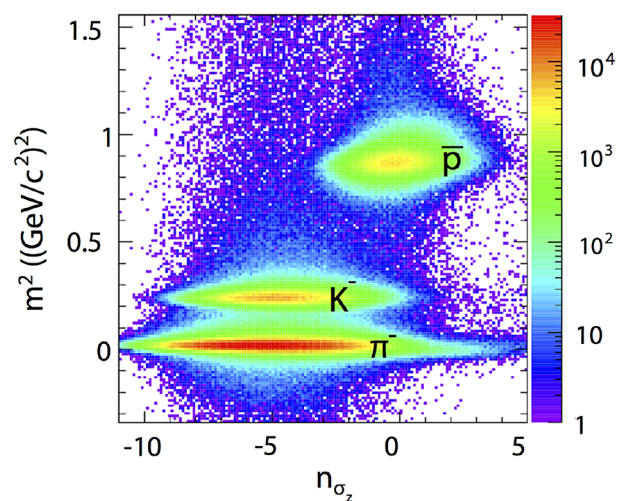


Fig. 3 (Color online) m^2 versus n_{σ_z} for negatively charged particles. Here $m^2 = (\mathbf{p}^2/c^2)(t^2c^2/L^2 - 1)$, where t and L are the time of flight and path length, respectively. c is the light velocity

3 Method

In this experiment, two-particle correlation function is defined as $\frac{A(k^*)}{B(k^*)}$, where $A(k^*)$ is the distribution of half of the relative momentum (k^*) measured for the correlated pairs from the same event. And $B(k^*)$ is the noncorrelated pairs from two different (mixed) events. Impurities in (anti)protons will reduce the observed correlation strength. We use the following equation for the pair purity correction:

$$CF_{corrected}(k^*) = \frac{CF_{measured}(k^*) - 1}{PairPurity(k^*)} + 1, \tag{2}$$

where $PairPurity(k^*)$ is the product of the purities for the two particles and $CF_{measured}(k^*)$ and $CF_{corrected}(k^*)$ are respectively the corrected and measured correlation functions.

Inside our (anti)proton sample, there are secondary (anti)protons that are indistinguishable from primordial ones. When considering resonances, one should distinct the short-lived ones (like Delta) from the long-lived ones (decaying electromagnetically or weakly, like Lambda). The latter give rise to the effect of residual correlations (due to small decay momenta) as discussed in the paper. Their decay lengths are huge and do not affect the measured invariant radius R_{pp} ; they reveal themselves only through the suppression parameter, x_{pp} , and through the residual correlation contributions. The short-lived resonances do not contribute to residual correlations (not only due to substantial decay momenta, but also due to short decay times comparable with the production time, thus not allowing for the FSI to be developed). The residual correlations are mainly from the p-Λ and Λ-Λ correlations or their antiparticle pairs. We need to consider the corresponding contributions when we fit our CF. Taking the two-proton correlation function as an example [44],

$$C_{inclusive}(k^*) = 1 + x_{pp}[C_{pp}(k^*; R_{pp}) - 1] + x_{p\Lambda}[C_{p\Lambda}(k^*; R_{p\Lambda}) - 1] + x_{\Lambda\Lambda}[C_{\Lambda\Lambda}(k^*) - 1], \tag{3}$$

where $C_{inclusive}(k^*)$ is the inclusive CF, and $C_{pp}(k^*; R_{pp})$ is the true proton-proton CF, which can be described by the Lednický and Lyuboshitz analytical model [37]. In this model, for given s-wave scattering parameters, the correlation function with FSI is calculated as the square of the properly symmetrized wave function averaged over the total pair spin and the distribution of relative distances of particle emission points in the pair rest frame. $C_{p\Lambda}(k^*; R_{p\Lambda})$ is the p-Λ CF from a theoretical calculation [37] which has explained experimental data well [39]. $C_{\Lambda\Lambda}(k^*)$ is from an experimental measurement corrected for misidentified Λ's [40]. R_{pp} and $R_{p\Lambda}$ are the invariant Gaussian radii [39] from

the proton-proton correlation and the proton-Λ correlation, respectively. Here they are assumed numerically to be the same. x_{pp} , $x_{p\Lambda}$, and $x_{\Lambda\Lambda}$ represent the relative contributions from pairs with both daughters from the primary collision, pairs with one daughter from the primary collision and the other one from a Λ decay, and pairs with both daughters from a Λ decay, respectively. THERMINATOR2 model can give such parameters [45]. $C_{p\Lambda}(k_{pp}^*) = \int C_{p\Lambda}(k_{p\Lambda}^*) T(k_{p\Lambda}^*, k_{pp}^*) dk_{p\Lambda}^*$, where $T(k_{p\Lambda}^*, k_{pp}^*)$ is a matrix that transforms $k_{p\Lambda}^*$ to k_{pp}^* [44].

The proton-proton correlation function, $C_{pp}(k^*; R_{pp})$ in Eq. 3, can be described by the Lednický and Lyuboshitz analytical model [37]. In this model, the correlation function is calculated as the square of the properly symmetrized wave function averaged over the total pair spin, S , and the distribution of relative distances (\mathbf{r}^*) of particle emission points in the pair rest frame, assuming 1/4 of the singlet and 3/4 of triplet states and a simple Gaussian distribution $dN/d^3\mathbf{r}^* \sim \exp(-\mathbf{r}^{*2}/4R_{pp}^2)$. Starting with the FSI weight of nucleons emitted with the separation \mathbf{r}^* and detected with the relative momentum \mathbf{k}^* ,

$$w(\mathbf{k}^*, \mathbf{r}^*) = |\psi_{-\mathbf{k}^*}^{S(+)}(\mathbf{r}^*) + (-1)^S \psi_{\mathbf{k}^*}^{S(+)}(\mathbf{r}^*)|^2/2, \tag{4}$$

where $\psi_{-\mathbf{k}^*}^{S(+)}(\mathbf{r}^*)$ is the equal-time ($t^* = 0$) reduced Bethe-Salpeter amplitude which can be approximated by the outer solution of the scattering problem [46]. This is

$$\psi_{-\mathbf{k}^*}^{S(+)}(\mathbf{r}^*) = e^{i\delta_c} \sqrt{A_c(\eta)} [e^{-ik^*r^*} F(-i\eta, 1, i\xi) + f_c(k^*) \frac{\tilde{G}(\rho, \eta)}{r^*}], \tag{5}$$

where $\eta = (k^* a_c)^{-1}$, $a_c = (57.5 \text{ fm})$ is the Bohr radius for two protons, $\rho = k^* r^*$, $\xi = \mathbf{k}^* \mathbf{r}^* + \rho$, $A_c(\eta)$ is the Coulomb penetration factor given by $A_c(\eta) = 2\pi\eta[\exp(2\pi\eta) - 1]^{-1}$, F is the confluent hypergeometric function, $\tilde{G}(\rho, \eta) = \sqrt{A_c(\eta)}[G_0(\rho, \eta) + iF_0(\rho, \eta)]$ is a combination of the regular (F_0) and singular (G_0) s-wave Coulomb functions,

$$f_c(k^*) = \left[\frac{1}{f_0} + \frac{1}{2} d_0 k^{*2} - \frac{2}{a_c} h(\eta) - ik^* A_c(\eta) \right]^{-1} \tag{6}$$

is the s-wave scattering amplitude renormalized by the Coulomb interaction, and $h(\eta) = \eta^2 \sum_{n=1}^{\infty} [n(n^2 + \eta^2)]^{-1} - C - \ln|\eta|$ (here $C \doteq 0.5772$ is the Euler constant). The dependence of the scattering parameters on the total pair spin, S , is omitted since only the singlet ($S = 0$) s-wave FSI contributes in the case of identical nucleons. The theoretical CF at a given k^* can be calculated as the average FSI weight $\langle w(\mathbf{k}^*, \mathbf{r}^*) \rangle$ obtained from the separation r^* , simulated according to the Gaussian law, and the angle between

the vectors \mathbf{k}^* and \mathbf{r}^* , simulated according to a uniform cosine distribution. This CF is subject to the integral correction [37] $-A_c(\eta)|f_c(k^*)|^2 d_0/(8\sqrt{\pi}R_{pp}^3)$ due to the deviation of the outer solution from the true wave function in the inner potential region. Considering that the emitting source has a net positive charge in Au+Au collisions, which influences the CF differently for proton and antiproton pairs, this effect is included in the consideration according to Ref. [47, 48].

4 Results and discussion

When we fit the proton–proton correlation function, only the radius is the free parameter, and we fixed $f_0 = 7.82$ fm and $d_0 = 2.78$ fm as they are well determined (from proton–proton elastic-scattering experiments [49]). While when we fit the antiproton–antiproton correlation function, the radius R , f_0 , and d_0 are treated as free parameters. In Fig. 4, we present the PID purity corrected CF for proton–proton pairs

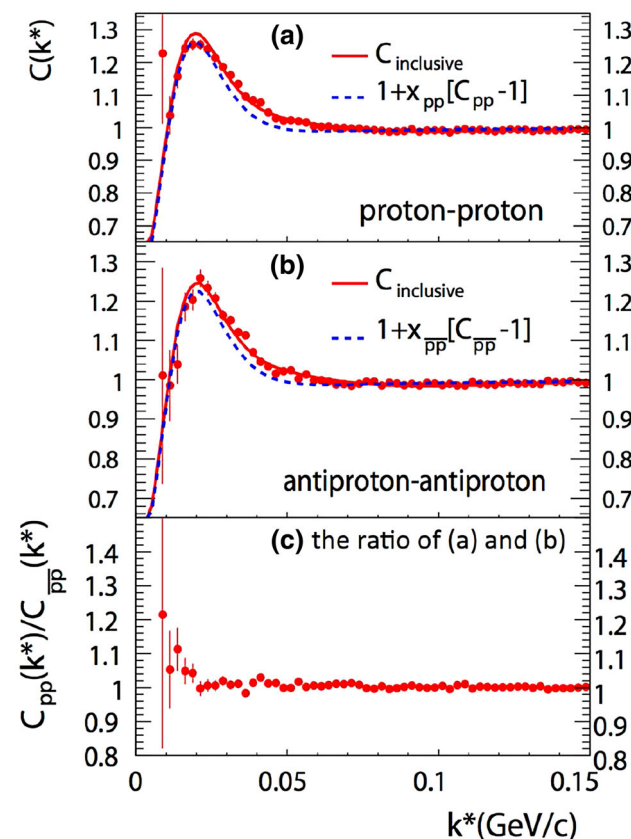


Fig. 4 (Color online) Proton–proton correlation (a), antiproton–antiproton correlation (b), and the ratio of the former to the latter (c). Errors are statistical only. The fits to the data with Eq. 3, $C_{\text{inclusive}}(k^*)$, are plotted as *solid lines*, and the term $1 + x_{pp}[C_{pp}(k^*; R_{pp}) - 1]$ is shown as *dashed lines*. The χ^2/NDF of the fit is 1.66 and 1.61 for a and b, respectively

(Fig. 4a) and antiproton–antiproton pairs (Fig. 4b), for 30–80% centrality of Au + Au collisions at center-of-mass energy of 200 GeV. The fit to the data is plotted as red solid lines, shown for $C_{\text{inclusive}}$, while the CF of pp contribution is shown as dashed lines. For proton–proton CF, $R_{pp} = 2.75 \pm 0.01$ fm; $\chi^2/\text{NDF} = 1.66$. For antiproton–antiproton CF, $R_{\bar{p}\bar{p}} = 2.80 \pm 0.02$ fm; $f_0 = 7.41 \pm 0.19(\text{stat}) \pm 0.36(\text{sys})$ fm; $d_0 = 2.14 \pm 0.27(\text{stat}) \pm 1.34(\text{sys})$ fm; $\chi^2/\text{NDF} = 1.61$. The proton–proton CF exhibits a maximum at k^* around 0.02 GeV, which is caused by the attractive S-wave interaction between the two protons and is consistent with previous measurements. The antiproton–antiproton CF shows an exact similar structure, indicating that the interaction between two antiprotons is also attractive. Figure 4c shows the ratio of the inclusive CF for proton–proton pairs to that of antiproton–antiproton pairs, and it is unity except for a very small k^* region where the error becomes large. This indicates that both proton–proton and antiproton–antiproton have the same strong interaction.

Table 2 presents strong interaction parameters f_0 and d_0 of the antiproton–antiproton interaction as well as prior measurements for nucleon–nucleon interactions [49, 50]. It is found that the f_0 and d_0 for the antiproton–antiproton interaction are consistent with the proton–proton interaction within errors.

5 Summary and outlook

Our STAR measurements on momentum correlation function of antiproton–antiproton pair from the RHIC–STAR detector provide quantitative parameters of scattering length and effective range for antiproton–antiproton interaction [51]. These parameters illustrate the strong interaction between antiprotons is attractive, which is the basis of the formation of complex antinuclei. The

Table 2 f_0 and d_0 of (anti)nucleon–(anti)nucleon interactions

	Proton–proton	Antiproton–antiproton
f_0 (fm)	7.82 ± 0.003	$7.41 \pm 0.19(\text{stat}) \pm 0.36(\text{sys})$
d_0 (fm)	2.78 ± 0.006	$2.14 \pm 0.27(\text{stat}) \pm 1.34(\text{sys})$
	Proton–neutron (triplet)	Neutron–neutron
f_0 (fm)	-5.425 ± 0.018	16.7 ± 0.38
d_0 (fm)	1.711 ± 0.053	2.78 ± 0.13
	Proton–neutron (singlet)	
f_0 (fm)	23.721 ± 0.02	
d_0 (fm)	2.658 ± 0.062	

parameters also provide input for describing the interaction among cold-trapped gases of antimatter ions, as in an ultracold environment, where s-wave scattering dominates and effective-range theory shows that the scattering length and effective range are parameters that suffice to describe elastic collisions [52]. The result provides a new quantitative verification of matter–antimatter symmetry in the important and ubiquitous context of the forces responsible for the binding of (anti)nuclei.

Finally, considering the relatively large error of the current data, possible future improvement on the measurement can be made by reducing the uncertainty from the $\Lambda - \Lambda$ CF ($C_{\Lambda-\Lambda}(k^*)$), which dominates our systematical error, with further accumulation of data. In addition, a similar effort of extracting f_0 and d_0 could also be repeated with (anti)proton CF [53] measured at the Large Hadron Collider, where the yield ratio of antiproton to proton is close to unity. In an additional way, the interaction between antiprotons could be also measured by antiproton–antiproton scattering, which could be realized in the future, by which f_0 and d_0 can be extracted by studying the s-wave scattering phase shift versus energy.

Acknowledgments We thank the whole collaborators of the STAR collaboration, especially for Dr. Ai-Hong Tang of BNL, the RHIC Operations Group, the Collider-Accelerator Department, and the RHIC Computing Facility at BNL.

References

- R.V. Reid, Local phenomenological nucleon–nucleon potentials. *Ann. Phys.* **50**, 411–448 (1968). doi:10.1016/0003-4916(68)90126-7
- R. Machleidt, I. Slaus, *J. Phys. G: Nucl. Part. Phys.* **27**, R 69 (2001). doi:10.1088/0954-3899/27/5/201
- A.B. Larionov, Antiproton–nucleus reactions at intermediate energies. *Nucl. Sci. Tech.* **26**, S20506 (2015). doi:10.13538/j.1001-8042/nst.26.S20506
- Z.Q. Feng, Nuclear dynamics induced by antiprotons. *Nucl. Sci. Tech.* **26**, S20512 (2015). doi:10.13538/j.1001-8042/nst.26.S2051
- C.M. Ko, L.W. Chen, V. Greco et al., Mean-field effects on matter and antimatter elliptic flow. *Nucl. Sci. Tech.* **24**, 050525 (2013). doi:10.13538/j.1001-8042/nst.2013.05.025
- Y.G. Ma, J.H. Chen, L. Xue, A brief review of antimatter production. *Front. Phys.* **7**, 637 (2012). doi:10.1007/s11467-012-0273-9
- Y.G. Ma, J.H. Chen, L. Xue et al., Hunting antimatter nuclei in ultrarelativistic heavy-ion collisions. *Nucl. Phys. News* **23**(1), 10–14 (2013). doi:10.1080/10619127.2012.738164
- Y.G. Ma, Detecting the anti-hypertriton and anti-helium-4 from the RHIC. *EPJ Web Conf.* **66**, 04020 (2014). doi:10.1051/epjconf/20146604020
- J.H. Chen, for the STAR Collaboration, Observation of hypertritons in Au+Au collisions at $\sqrt{s_{NN}} = 200$ GeV. *Nucl. Phys. A* **830**, 761c–764c (2009). doi:10.1016/j.nuclphysa.2009.10.001
- B.I. Abelev, STAR Collaboration, et al., Observation of an antimatter hypernucleus. *Science* **328**, 58 (2010). doi:10.1126/science.1183980
- H. Agakishiev, STAR Collaboration, et al., Observation of the antimatter helium-4 nucleus. *Nature* **473**, 353–356 (2011). doi:10.1038/nature10079
- L. Xue, for the STAR Collaboration, Observation of the antimatter helium-4 nucleus at the RHIC. *J. Phys. G: Nucl. Part. Phys.* **38**, 124072 (2011). doi:10.1088/0954-3899/38/12/124072
- J. Adam, ALICE Collaboration, Precision measurement of the mass difference between light nuclei and anti-nuclei. *Nat. Phys.* **11**, 811–814 (2015). doi:10.1038/NPHYS3432
- S. Ulmer et al., High-precision comparison of the antiproton-to-proton charge-to-mass ratio. *Nature* **524**, 196–198 (2015). doi:10.1038/nature14861
- K.A. Olive, Particle Data Group, et al., Review of particle physics. *Chin. Phys. C* **38**, 090001–091676 (2014). doi:10.1088/1674-1137/38/9/090001
- J. Adams, M.M. Aggarwal, Z. Ahammed et al., Experimental and theoretical challenges in the search for the quark–gluon plasma: The STAR Collaboration’s critical assessment of the evidence from RHIC collisions. *Nucl. Phys. A* **757**, 102–183 (2005). doi:10.1016/j.nuclphysa.2005.03.085
- K. Adcox, S.S. Adler, S. Afanasiev et al., Formation of dense partonic matter in relativistic nucleus–nucleus collisions at RHIC: experimental evaluation by the PHENIX collaboration. *Nucl. Phys. A* **757**, 184–283 (2005). doi:10.1016/j.nuclphysa.2005.03.086
- Y.G. Ma, Frontier of high-energy nuclear physics: exploring the quark–gluon plasma. *Mod. Phys.* **25**(5), 27–34 (2013) (in Chinese)
- R. Hanbury-Brown, R.Q. Twiss, A new type of interferometer for use in radio astronomy. *Philos. Mag.* **45**, 663–682 (1954). doi:10.1080/14786440708520475
- G.I. Kopylov, Like particle correlations as a tool to study the multiple production mechanism. *Phys. Lett. B* **50**, 472–474 (1974). doi:10.1016/0370-2693(74)90263-9
- G.I. Kopylov, M.I. Podgoretsky, Interference of two-particle states in elementary-particle physics and astronomy. *Sov. Phys. JETP* **42**, 211–214 (1975)
- M.I. Podgoretsky, Interference correlations of identical pions. *Sov. J. Part. Nucl. Theory* **20**, 266–282 (1989)
- M. Schellekens et al., Hanbury Brown Twiss effect for ultracold quantum gases. *Science* **310**, 648–651 (2005). doi:10.1126/science.1118024
- H. Kiesel, A. Renz, F. Hasselbach, Observation of Hanbury-Brown Twiss anticorrelations for free electrons. *Nature* **418**, 392–394 (2002). doi:10.1038/nature00911
- T. Rom et al., Free fermion antibunching in a degenerate atomic Fermi gas released from an optical lattice. *Nature* **444**, 733–736 (2006). doi:10.1038/nature05319
- G. Goldhaber, S. Goldhaber, W. Lee, A. Pais, Influence of Bose–Einstein statistics on the antiproton–proton annihilation process. *Phys. Rev.* **120**, 300–312 (1960). doi:10.1103/PhysRev.120.300
- M. Gyulassy, S.K. Kauffmann, L.W. Wilson, Pion interferometry of nuclear collisions. I. Theory. *Phys. Rev. C* **20**, 2267–2292 (1979). doi:10.1103/PhysRevC.20.2267
- H.D. Boal, C.K. Gelbke, B.K. Jennings, Intensity interferometry in subatomic physics. *Rev. Mod. Phys.* **62**(3), 553–602 (1990). doi:10.1103/RevModPhys.62.553
- R. Lednický, Correlation femtoscopy of multiparticle processes. *Phys. At. Nucl.* **67**, 72–82 (2004). doi:10.1134/1.1644010
- W.G. Lynch et al., Formation and decay of a localized region of high excitation in heavy-ion-induced reactions. *Phys. Rev. Lett.* **51**, 1850 (1983). doi:10.1103/PhysRevLett.51.1850
- Y.G. Ma et al., Surveying the nucleon–nucleon momentum correlation function in the framework of quantum molecular dynamics model. *Phys. Rev. C* **73**, 014604 (2006). doi:10.1103/PhysRevC.73.014604

32. Y.G. Ma et al., Nucleon-nucleon momentum correlation function for light nuclei. Nucl. Phys. A **790**, 299c (2007). doi:[10.1016/j.nuclphysa.2007.03.146](https://doi.org/10.1016/j.nuclphysa.2007.03.146)
33. M. Lisa, S. Pratt, R. Soltz, U. Wiedemann, Femtoscopy in relativistic heavy ion collisions: two decades of progress. Ann. Rev. Nucl. Part. Sci. **55**, 357–402 (2005). doi:[10.1146/annurev.nucl.55.090704.151533](https://doi.org/10.1146/annurev.nucl.55.090704.151533)
34. Y.G. Ma, D.Q. Fang, X.Y. Sun et al., Different mechanism of two-proton emission from proton-rich nuclei ^{23}Al and ^{22}Mg . Phys. Lett. B **743**, 306 (2015). doi:[10.1016/j.physletb.2015.02.066](https://doi.org/10.1016/j.physletb.2015.02.066)
35. D.Q. Fang, Y.G. Ma, X.Y. Sun et al., Proton-proton correlations in distinguishing the two-proton emission mechanism of ^{23}Al and ^{22}Mg . Phys. Rev. C **94**, 044621 (2016). doi:[10.1103/PhysRevC.94.044621](https://doi.org/10.1103/PhysRevC.94.044621)
36. S.E. Koonin, Proton pictures of high-energy nuclear collisions. Phys. Lett. B **70**, 43–47 (1977). doi:[10.1016/0370-2693\(77\)90340-9](https://doi.org/10.1016/0370-2693(77)90340-9)
37. L. Rednický, V.L. Lyuboshitz, Influence of final-state interaction on correlations of two particles with nearly equal momenta. Sov. J. Nucl. Phys. **35**, 770–788 (1982)
38. R. Lednický, Notes on correlation femtoscopy. Phys. At. Nucl. **71**, 1572–1578 (2008). doi:[10.1134/S1063778808090123](https://doi.org/10.1134/S1063778808090123)
39. J. Adams, STAR Collaboration, et al., Proton- Λ correlations in central Au+Au collisions at $\sqrt{s_{\text{NN}}} = 200$ GeV. Phys. Rev. C **74**, 064906 (2006). doi:[10.1103/PhysRevC.74.064906](https://doi.org/10.1103/PhysRevC.74.064906)
40. L. Adamczyk, STAR Collaboration, et al., $\Lambda - \Lambda$ correlation function in Au+Au collisions at $\sqrt{s_{\text{NN}}} = 200$ GeV. Phys. Rev. Lett. **114**, 022301 (2015). doi:[10.1103/PhysRevC.74.064906](https://doi.org/10.1103/PhysRevC.74.064906)
41. M. Anderson et al., The STAR time projection chamber: a unique tool for studying high multiplicity events at RHIC. Nucl. Instrum. Methods Phys. Res. A **499**, 659–678 (2003). doi:[10.1016/S0168-9002\(02\)01964-2](https://doi.org/10.1016/S0168-9002(02)01964-2)
42. W.J. Llope, for the STAR Collaboration, Multigap RPCs in the STAR experiment at RHIC. Nucl. Instrum. Methods Phys. Res. A **661**, s110–s113 (2012). doi:[10.1016/j.nima.2010.07.086](https://doi.org/10.1016/j.nima.2010.07.086)
43. Y.-F. Xu, J.-H. Chen, Y.-G. Ma, A.-H. Tang, Z.-B. Xu, Y.-H. Zhu, Physics performance of the STAR zero degree calorimeter at relativistic heavy ion collider. Nucl. Sci. Tech. **27**, 126 (2016). doi:[10.1007/s41365-016-0129-z](https://doi.org/10.1007/s41365-016-0129-z)
44. H. Zbroszczyk, Studies of baryon-baryon correlations in relativistic nuclear collisions registered at the STAR experiment. Ph. D Thesis, Warsaw University of Technology (2008)
45. M. Chojnacki, A. Kisiel, W. Florkowski, W. Broniowski, THERMINATOR 2: THERMal heavy Ion generATOR 2. Comput. Phys. Commun. **183**, 746–773 (2012). doi:[10.1016/j.cpc.2011.11.018](https://doi.org/10.1016/j.cpc.2011.11.018)
46. L.D. Landau, E.M. Lifshitz, *Quantum Mechanics* (Nauka, Moscow, 1974)
47. B. Erazmus et al., Influence of the emitting nucleus on the light-particle correlation function. Nucl. Phys. A **583**, 395–400 (1995). doi:[10.1016/0375-9474\(94\)00693-H](https://doi.org/10.1016/0375-9474(94)00693-H)
48. R. Lednický, Finite-size effect on two-particle production in continuous and discrete spectrum. Phys. Part. Nucl. **40**, 307–352 (2009). doi:[10.1134/S1063779609030034](https://doi.org/10.1134/S1063779609030034)
49. L. Mathelitsch, B.J. VerWest, Effective range parameters in nucleon-nucleon scattering. Phys. Rev. C **29**, 739–745 (1984). doi:[10.1103/PhysRevC.29.739](https://doi.org/10.1103/PhysRevC.29.739)
50. I. Šlaus, Y. Akaishi, H. Tanaka, Neutron-neutron effective range parameters. Phys. Rep. **173**, 257–300 (1989). doi:[10.1016/0370-1573\(89\)90127-0](https://doi.org/10.1016/0370-1573(89)90127-0)
51. L. Adamczyk, STAR Collaboration, et al., Measurement of interaction between antiprotons. Nature **527**, 345–348 (2015). doi:[10.1038/nature15724](https://doi.org/10.1038/nature15724)
52. N.F. Mott, H.S.W. Massey, *The Theory of Atomic Collisions* (Oxford University Press, Oxford, 1965)
53. J. Adam, ALICE Collaboration, et al., One-dimensional pion, kaon, and proton femtoscopy in Pb-Pb collisions at $\sqrt{s_{\text{NN}}} = 2.76$ TeV. Phys. Rev. C **92**, 054908 (2015). doi:[10.1103/PhysRevC.92.054908](https://doi.org/10.1103/PhysRevC.92.054908)